Simulation study of laser diode based GaInP/AlGaInP structure

L. Abdelali[a], Z. Abed[a], and A. Bouguenna[b],

[a]*Applied Materials Laboratory, Research Center, Sidi Bel Abbes University, 22000, Algeria.*
e-mail: laid.abdelali@univ-sba.dz; laidabdelali@gmail.com
[b]*Department of Electronics, Faculty of Electrical Engineering, University of Sciences & Technology of Oran (USTO-MB), 31000, Oran, Algeria.*

Received 6 September 2025; accepted 8 May 2026

In this work, we investigate the energy levels and optimization of intrinsic parameters (such as number and width of wells, potential barrier width, refractive index, etc.) and extrinsic parameters (including temperature and pressure) in a laser diode based on the GaInP/AlGaInP structure. The computational techniques employed include the pseudo-empirical potential method to determine the electronic band structures and a graphical method for optimization. Our results are consistent with experimental and theoretical results.

Keywords: Laser diode; semi-conductor; GaInP/AlGaInP; pseudo-potential.

DOI: https://doi.org/10.31349/RevMexFis.72.051005

1. Introduction

AlGaInP laser diodes (LDs) are used in a variety of digital equipment, such as MO/CD/DVD optical pickup units, laser printers and barcode scanners [1]. AlGaInP is a quaternary alloy and involves three binary compounds: GaP, InP and AlP.

The active material for visible light-emitting diodes (LEDs) has long been nitrogen-doped GaP. We shall only take into consideration GaP as the sole indirect-gap semiconductor (with X–L–Γ ordering of the conduction-band minima) that is devoid of Al.

Since it is the substrate for the majority of optoelectronic devices operating at the 1.55 μm communications wavelength, InP is a direct-gap semiconductor of significant technological importance. Among III–V compound semiconductors, AlP is undoubtedly the most "exotic" and least researched because of its large direct band gap.

Among non-nitride III–V semiconductors, the GaInP alloy exhibits some of the largest direct band gaps. Additionally, $Ga_{0.51}In_{0.49}P$ ($E_g = 1.9$ eV at 300 K) is lattice-matched to GaAs, making it a desirable material for wide-band-gap GaAs-based quantum-well devices such as red diode lasers [2].

Extensive studies have been performed on GaInP/AlGaInP structures, including semiconductor disk lasers (SDLs) [3], red lasers [4], microdisk lasers for biophotonics applications [5], red light-emitting diodes [6], and laser diodes [7], among others.In this paper, we report a study of the energy levels and the optimization of intrinsic and extrinsic parameters in a laser diode based on the GaInP/AlGaInP structure.

2. Results and Discussions

2.1. Adjustment of the Form Factors of the Three Binary Elements

The form factors (symmetrical and anti-symmetrical) of the various binary compounds (GaP, InP, and AlP) to which the quaternary compound AlGaInP refers are adjusted by the *Zajust* program, based on the nonlinear least-squares method. The injected parameters are iteratively optimized until the mean square root of the variation (RMS) is minimized. Table I illustrates the different types of parameters.

2.2. Electronic Band Structure of the Two Binary Compounds

The energy band structures in wave vector space (K), resulting from the data presented in Table II, for the three binary compounds GaP, InP and AlP are shown in Fig 1.

TABLE I. Form factors and lattice constants of the binary compounds.

Materials	Form Factors						Lattice constant A′	Lattice constant (u.a)
	$V^s(3)$	$V^s(8)$	$V^s(11)$	$V^a(3)$	$V^a(4)$	$V^a(11)$		
GaP	-0.211024	0.030000	0.072296	0.132573	0.070000	0.020000	5.451	10.30103
InP	-0.213877	0.000000	0.075010	0.088777	0.060000	0.030000	5.869	10.090953
AlP	-0.202663	0.040000	0.080000	0.133288	0.0880571	0.015000	5.450	10.3009

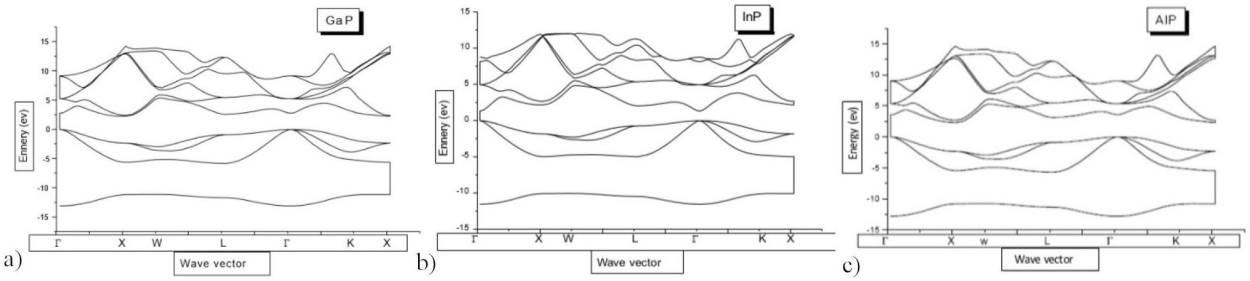

FIGURE 1. Structures of energy bands of GaP, InP and AlP.

TABLE II. Comparison of calculated and experimental energy gaps for the three binary compounds.

Materials	Energy Gaps (eV)					
	E_g^Γ		E_g^X		E_g^L	
	Exp, or other theoretical work	Our Simulation	Exp, or another work	Our Simulation	Exp, or another work	Our Simulation
GaP	$2.79^{a)}$	2.77968	$2.27^{a)}$	2.25924	$2.70^{a)}$	2.59957
InP	$1.34^{b)}$	1.34387	$2.20^{b)}$	2.19608	$2.04^{b)}$	2.04482
AlP	$3.61^{c)}$	3.57380	$2.31^{c)}$	2.3095	$3.12^{c)}$	3.12952

$^{a)}$ [5]. $^{b)}$ [9]. $^{c)}$ [10].

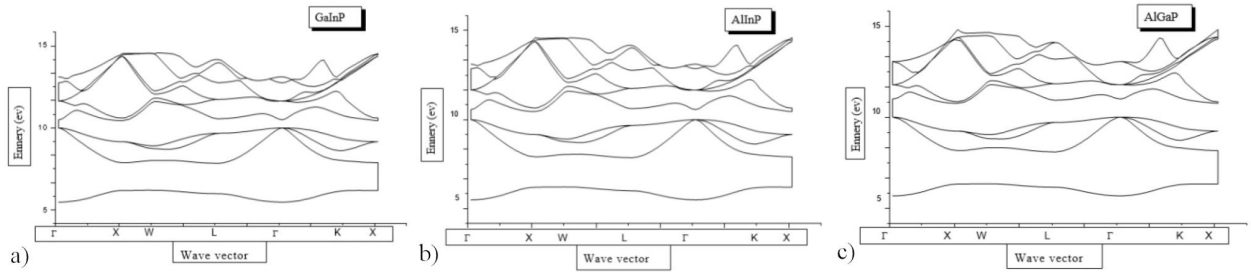

FIGURE 2. Structures of energy bands of $Ga_{0.51}In_{0.49}P$, $Al_{0.51}In_{0.49}P$, $Al_{0.51}Ga_{0.49}P$.

2.3. Electron band structure of the three ternary compounds with disorder

Figure 2 illustrates the energy band structures calculated using (EPM) of the three ternary compounds: $Ga_xIn_{1-x}P$, $Al_xIn_{1-x}P$ and $Al_xGa_{1-x}P$, taking into account compositional disorder (but not volume disorder) for $x = 0.51$.

Figure 3 illustrates the variations in energy gaps $E_{\Gamma\Gamma}$, $E_{\Gamma X}$ and $E_{\Gamma L}$ for $Ga_xIn_{1-x}P$ for different x concentration .from there . In this context, where p is the tuning parameter that is deliberately varied, (while setting the composition x to a specific valueeach time), until the parameters of the $Ga_xIn_{1-x}P$ ternary compound curve approximate experimental results and other theoretical calculations. Two values of the tuning parameter were considered:

- $p = 0$, corresponding to the traditional Virtual Crystal Approximation (VCA).
- $p = 0.65$, corresponding to the improved VCA model.

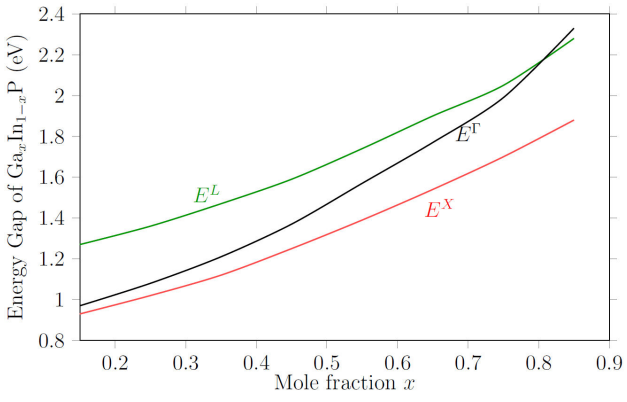

FIGURE 3. Gaps $Ga_xIn_{1-x}P$ according to x.

The results the calculation oh the variation of the gap $E_{\Gamma\Gamma}$ according to the concentration x .

The calculations of the different energy gaps (E_g^Γ, E_g^X, and E_g^L) by EPM (not taking into account the disorder ef-

TABLE III. Energy gaps E_g^Γ, E_g^X . E_g^L of $Ga_xIn_{1-x}P$ with x $(0 < x < 1)$.

Materials	Energy Gaps (eV)		
$Ga_xIn_{1-x}P$	E_g^Γ	E_g^X	E_g^L
$x = 0.15$	0.97230	0.92587	1.27417
$x = 0.30$	1.15682	1.08416	1.42010
$x = 0.45$	1.39213	1.27360	1.60079
$x = 0.60$	1.66644	1.48400	1.80635
$x = 0.75$	1.98112	1.71778	2.03737
$x = 0.90$	2.35735	1.98351	2.30736

TABLE IV. Energy gaps E_g^Γ, E_g^X and E_g^L of $Al_xIn_{1-x}P$ with x $(0 < x < 1)$.

Materials	**Energy Gaps (eV)**		
$Al_xIn_{1-x}P$	E_g^Γ	E_g^X	E_g^L
$x = 0.15$	0.949042	0.92831	1.25342
$x = 0.30$	1.21408	1.08594	1.47164
$x = 0.45$	1.55345	1.2798	1.74500
$x = 0.60$	1.94812	1.49742	2.06038
$x = 0.75$	2.39955	1.73705	2.41441
$x = 0.90$	2.93780	2.01676	2.82808

TABLE V. Energy gaps E_g^Γ, E_g^X and E_g^L of $Al_xGa_{1-x}P$ with x $(0 < x < 1)$.

Materials	Energy Gaps (eV)		
$Al_xGa_{1-x}P$	E_g^Γ	E_g^X	E_g^L
$x = 0.15$	2.75683	2.25742	2.57957
$x = 0.30$	2.83614	2.26369	2.64906
$x = 0.45$	2.93908	2.27138	2.73962
$x = 0.60$	3.05895	2.28026	2.84548
$x = 0.75$	3.19587	2.28865	2.96695
$x = 0.90$	3.35887	2.29798	3.11253

fect), for different gallium concentrations $0 \leq x \leq 1$ of the three ternary alloys: $Ga_xIn_{1-x}P$, $Al_xIn_{1-x}P$, and $Al_xGa_{1-x}P$ are given in Tables III, IV and V.

2.4. Electronic Band Structure of the Three Ternaries with Disorder

Figure 4 illustrates the EPM energy band structures of the three ternaries : $Ga_xIn_{1-x}P$, $Al_xIn_{1-x}P$ and $Al_xGa_{1-x}P$, taking into account compositional disorder (but not the bulk disorder) for $x = 0.51$.

In Fig. 4a) and 4b), the valence band maximum is the zero energy reference. These two figures show that the maximum

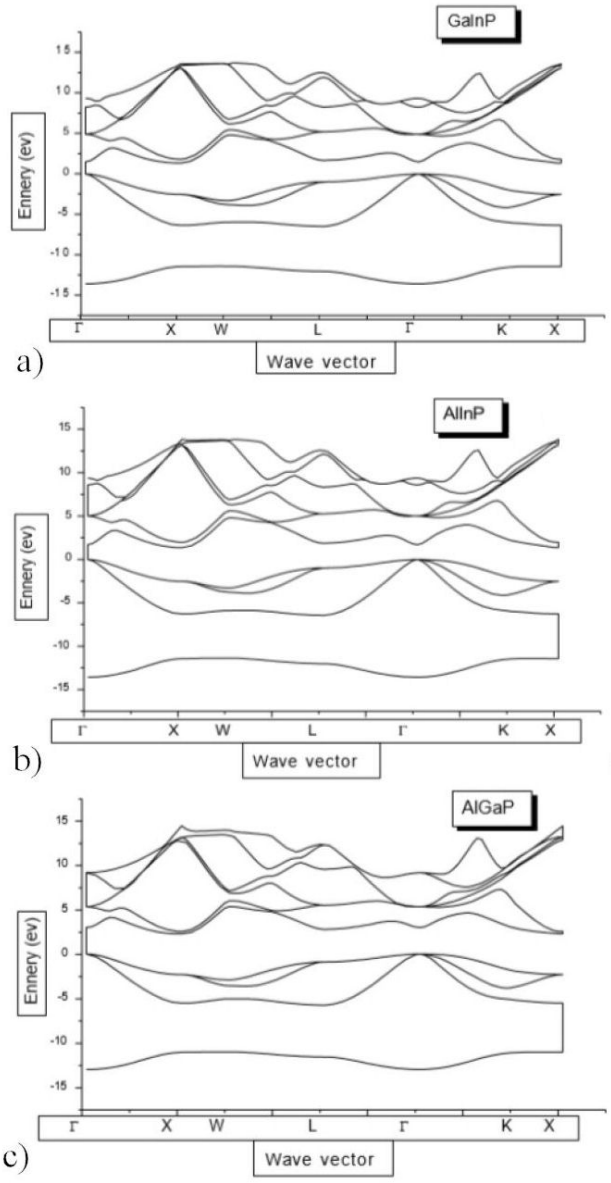

FIGURE 4. Energy band structures: $Ga_{0.51}In_{0.49}P$, $Al_{0.51}In_{0.49}P$ and $Al_{0.51}Ga_{0.49}P$.

of the valence band is at the point Γ that the conduction band minimum is also located at Γ. The ternary alloys $Ga_{0.51}In_{0.49}P$ and $Al_{0.51}In_{0.49}P$ are at direct gap, $E_{\Gamma\Gamma}$.

In Fig. 4c), where the valence band maximum is at point Γ and the conduction band minimum is at point L. the conduction band minimum is at point Γ, the ternary $Al_xGa_{1-x}P$ alloy is at indirect gap $E_{\Gamma L}$.

Figure 5 illustrates, respectively, the variations in the energy gaps E_g^Γ, E_g^X, and E_g^L for $Ga_xIn_{1-x}P$, $Al_xIn_{1-x}P$, and $Al_xGa_{1-x}P$ for different x concentrations.

Polynomial interpolation of the curves representing variations in gaps as a function of concentration x, which gives rise to leading to Eqs. (1)–(9) below:

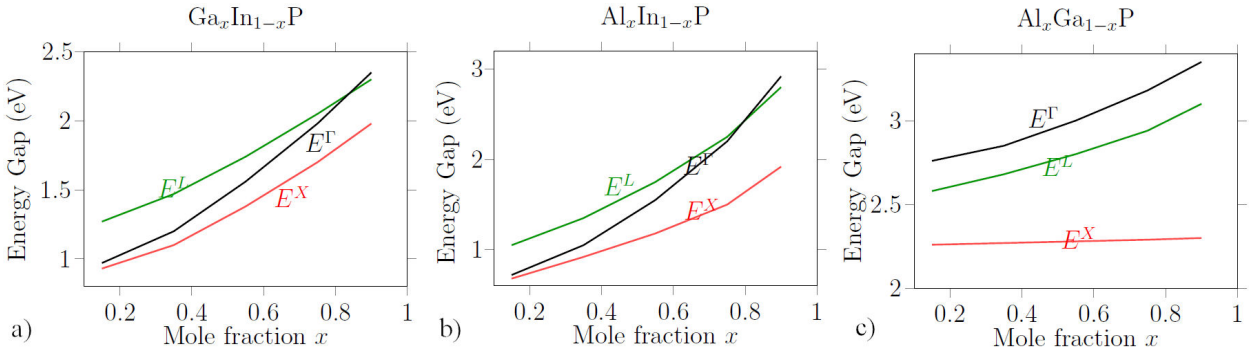

FIGURE 5. Gaps of $Ga_xIn_{1-x}P$, $Al_xIn_{1-x}P$ and $Al_xGa_{1-x}P$ as a function of x.

for $Ga_xIn_{1-x}P$

$$E_g^\Gamma = 0.834 + 0.773x + 1.017x^2. \quad (1)$$

$$E_g^X(x) = 0.790 + 0.817x + 0.653x^2. \quad (2)$$

$$E_g^L(x) = 1.155 - 0.691x + 0.651x^2. \quad (3)$$

for $Al_xIn_{1-x}P$

$$E_g^\Gamma = 0.746 + 1.134x + 1.440x^2. \quad (4)$$

$$E_g^X = 0.795 + 0.788x + 0.630x^2. \quad (5)$$

$$E_g^L = 1.076 + 1.018x + 1.028x^2. \quad (6)$$

for $Al_xGa_{1-x}P$

$$E_g^\Gamma = 2.695 + 0.339x + 0.439x^2. \quad (7)$$

$$E_g^X = 2.250 + 0.03x + 0.014x^2. \quad (8)$$

$$E_g^L = 2.527 + 0.289x + 0.400x^2. \quad (9)$$

where p is the tuning parameter which is deliberately varied (each time setting the composition x to a precise value) until the curvature parameters of the $Ga_xIn_{1-x}P$ sent ternary are close, with reference to experimental and other theoretical calculations. We have taken $p = 0$ (traditional VCA), and $p = 0.65$, $p = 0.36$ (improved VCA), the results of the calculation of the E_g^Γ gap variation with a concentration x are shown in Tables VI, VII and VIII.

TABLE VI. Energy gap $E_{\Gamma\Gamma}$ as a function of x for classic VCA ($p = 0$): $Ga_xIn_{1-x}P$.

x	0.31	0.49	0.52	0.68	0.76	0.91
$E_{\Gamma\Gamma}$	1.538	1.895	1.912	2.197	2.374	2.603

TABLE VII. Energy gap $E_{\Gamma\Gamma}$ as a function of x for improved VCA ($p = 0.65$): $Ga_xIn_{1-x}P$.

x	0.31	0.49	0.52	0.68	0.76	0.91
$E_{\Gamma\Gamma}$	1.042	1.354	1.372	1.690	1.922	2.283

TABLE VIII. Energy gap $E_{\Gamma\Gamma}$ as a function of x for improved VCA ($p = 0.36$): $Ga_xIn_{1-x}P$.

x	0.31	0.49	0.52	0.68	0.76	0.91
$E_{\Gamma\Gamma}$	1.265	1.597	1.612	1.916	2.125	2.425

The gap variations with a concentration x for the 2 types of VCA (conventional and improved), for $Ga_xIn_{1-x}P$ without taking into account the volume effect.

After recording the $E_{\Gamma\Gamma}$ gap, we plotted its variation as a function of concentration x to determine its equation by polynomial interpolation, fit the curves, and thus deduce the curvature parameters c. Figure 6 shows the representative curves of $E_{\Gamma\Gamma}$ gap variation with x fraction for the 2 cases of VCA (conventional and improved) for $Ga_xIn_{1-x}P$, polynomial interpolation of the representative curves of $E_{\Gamma\Gamma}$ gap variation with x gave the following polynomial equations:

For classic VCA ($p = 0$):

$$E_{\Gamma\Gamma} = 0.999 + 1.803x + 0.022x^2. \quad (10)$$

For the improved VCA ($p = 0.65$):

$$E_{\Gamma\Gamma} = 0.787 + 0.461x + 1.328x^2. \quad (11)$$

For the improved VCA ($p = 0.36$):

$$E_{\Gamma\Gamma} = 0.882 + 1.059x + 0.725x^2. \quad (12)$$

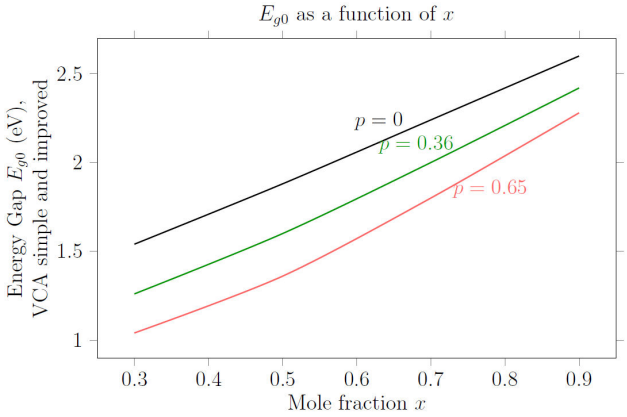

FIGURE 6. Gap versus x curves $E_{\Gamma\Gamma}$: conventional and improved VCA, for $Ga_xIn_{1-x}P$.

TABLE XIX. Compares the calculated and measured $E_{\Gamma\Gamma}$ curvature parameters of $Ga_xIn_{1-x}P$.

Our curvature parameter calculated by:	Result of other works
EPM and VCA classic (p=0) : -0.022	-0.07^d
EPM and VCA enhanced (p=0.65) : 1.328	–
EPM and VCA enhanced (p=0.36) : 0.725	0.72^d (p=0.22)

^{d}[11].

These $E(x)$ equations are of the form $a + bx + cx^2$, where c represents the curvature parameter of $Ga_xIn_{1-x}P$. Table XIX compares the calculated and measured $E_{\Gamma\Gamma}$ curvature parameters of $Ga_xIn_{1-x}P$, clearly showing that for $p = 0.36$ Eq. (12), the $Ga_xIn_{1-x}P$ gap is one curvature parameter and close to the experimental.

2.5. Electronic band structure of $Al_xGa_yIn_{1-x-y}P$ without orders

Figure 7 illustrates the energy band structure by EPM of $Al_xGa_yIn_{1-x-y}P$ taking into account no compositional disorder (but not volume disorder) for $y = 0.3$.

Calculations of the different energy gaps (E_g^Γ, E_g^X, E_g^L) by EPM (not taking into account the disorder effect) for different concentrations $0 \leq y \leq 0.4$ of the quaternary alloys $Al_{0.5}Ga_yIn_{0.5-y}P$ are given in Table X.

Figure 8 shows the respective variations in energy gaps for $Al_{0.5}Ga_yIn_{0.5-y}P$, for different y concentrations.

Polynomial interpolation of the curves representing variations in gaps as a function of concentration y, which gives rise to the following equations,

$$E_g^\Gamma = 0.771 + 4.988y + 0.383y^2, \quad (13)$$

$$E_g^X = 0.879 + 2.945y + 0.383y^2, \quad (14)$$

$$E_g^L = 1.409 + 3.395y + 0.258y^2. \quad (15)$$

We conclude that the improved VCA used to calculate the gap curvature parameter of $Ga_xIn_{1-x}P$ gives good results that are in almost total agreement with those obtained from experiment, which is not the case with the classical VCA, which does not faithfully reflect the results of these parameters.

Optimization of intrinsic and extrinsic physical parameters of structures $Ga_xIn_{1-x}P$/AlGaInP.

2.6. Optimization using the graphical method

2.6.1. Mesh mismatches and well constraints

Based on the matching condition between the materials of the active layers in the $Ga_xIn_{1-x}P$ quantum-well laser structure on the AlGaInP substrate, illustrated in Fig. 9, the evolution of $\Delta a/a_{\text{AlGaInP}}$ (quantifying the constraint in %) with the gallium (Ga) concentration for the $Ga_xIn_{1-x}P$ structure is such that:

$$\frac{\Delta a}{a_{\text{AlGaInP}}} = \frac{-0.4182x + 0.243}{5.626}, \quad (16)$$

of $Ga_xIn_{1-x}P/Al_{0.38}Ga_{0.21}In_{0.41}P$.

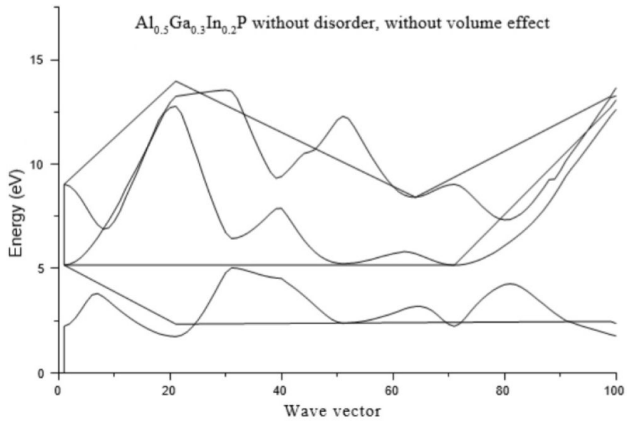

FIGURE 7. Energy band structures: $Al_{0.5}Ga_{0.3}In_{0.2}P$.

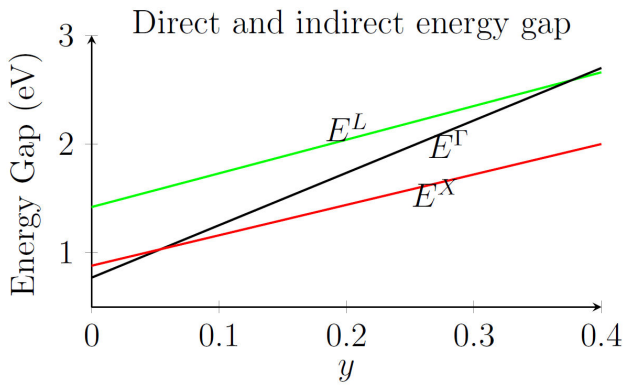

FIGURE 8. Gaps of $Al_{0.5}Ga_yIn_{0.5-y}P$ as a function of y.

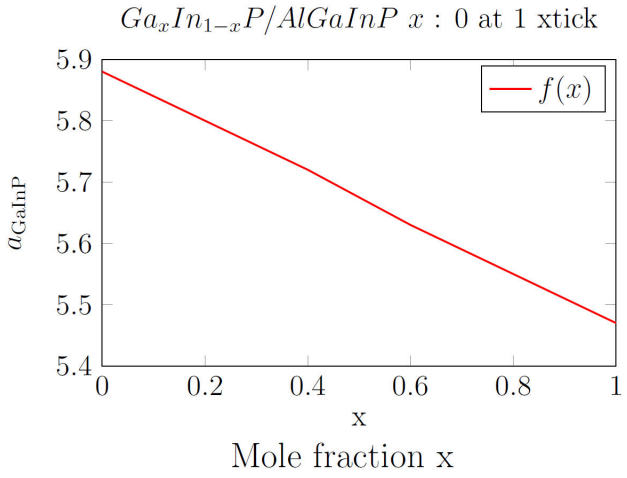

FIGURE 9. GaInP on AlGaInP matching condition.

TABLE X. Energy gaps E_g^{Γ}, E_g^{X}, E_g^{L} as a function of concentration y: $Al_{0.5}Ga_yIn_{0.5-y}P$.

y	0	0.05	0.1	0.15	0.2	0.25	0.3	0.35	0.4
E_g^{Γ}	0.7723	1.0209	1.2676	1.5121	1.7548	1.9955	2.2344	2.4712	2.7062
E_g^{X}	0.8794	1.0261	1.1715	1.3156	1.4584	1.5999	1.7400	1.8788	2.0162
E_g^{L}	1.4103	1.5785	1.7435	1.9052	2.0636	2.2187	2.3704	2.5189	2.6640

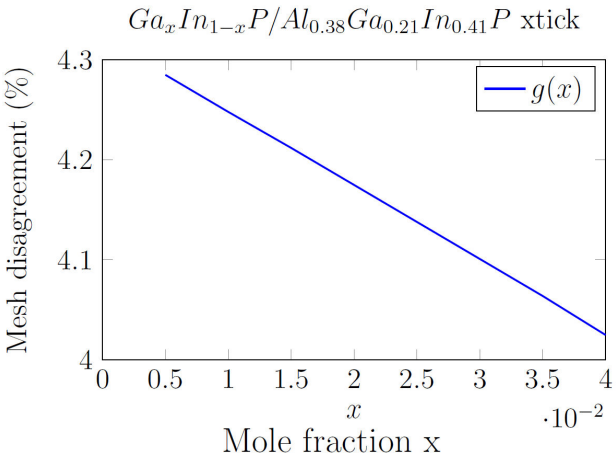

FIGURE 10. $\Delta a/a_{\text{AlGaInP}}$ as a function of x ($Ga_xIn_{1-x}P$).

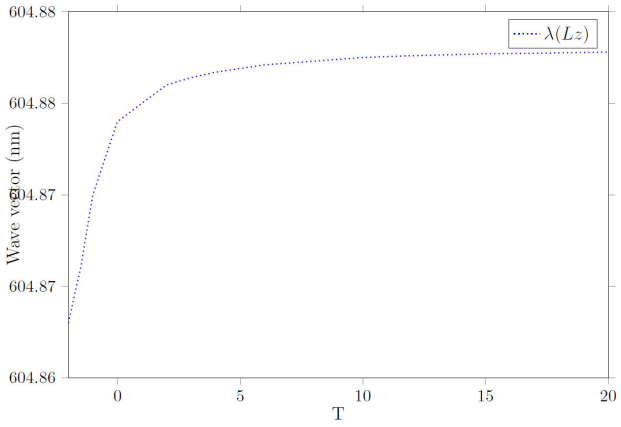

FIGURE 11. Wavelength variation as a function of well width for gallium concentrations in the active layer.

2.6.2. *Wave length*

We will calculate the wavelength emitted by the diode using the ternary $Ga_xIn_{1-x}P$ as an active layer (for $x = 0.5$), and the quaternary $Al_{0.31}Ga_{0.21}In_{0.48}P$ as a barrier. We also study the influence of temperature on the emission wavelength for a given well width.

a) Wavelength as a function of well width

A quantum-well laser is obtained when the active region has a dimension of less than 20 nm (the well width) [10].

We have the following equation, which gives the wavelength as a function of the quantum well width (L_z) [9]:

$$\lambda_n = \frac{1.24}{E_g + E_{cn} + E_{vn}} \ (\mu m), \tag{17}$$

E_{cn} and E_{vn} are given by the following approximate equations,

$$E_{cn} = (n+1)\frac{\Pi}{\sqrt{2m_c}\,L}, \tag{18}$$

$$E_{vn} = (n+1)\frac{\Pi}{\sqrt{2m_v}\,L}. \tag{19}$$

Figure 11 shows that the wavelength increases with the width of the well. This increase is very rapid at first, then becomes slower and slower, until it reaches zero. Thus, when the well width increases from 9 to 10 nm, the wavelength increases by only 0.25%. So a well width of 9 nm can be used satisfactorily for a wavelength greater than 604 nm.

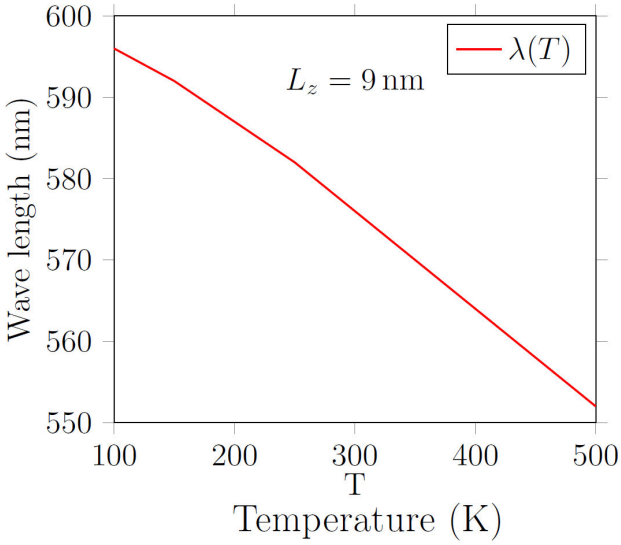

FIGURE 12. Wavelength variation as a function of temperature.

b) Wavelength as a function of temperature

Since temperature affects the energy gap, it also has an influence on wavelength. To study this influence, we use the VARSHNI model.

Figure 12 shows that wavelength decreases significantly with temperature. When the temperature rises from 100 to 400 K, the wavelength decreases by only 2.45%, so the influence of temperature is remarkable.

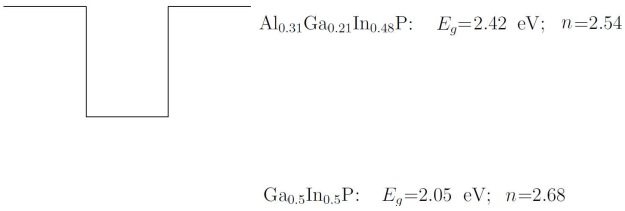

FIGURE 13. Represents the structure with their gap and refractive index.

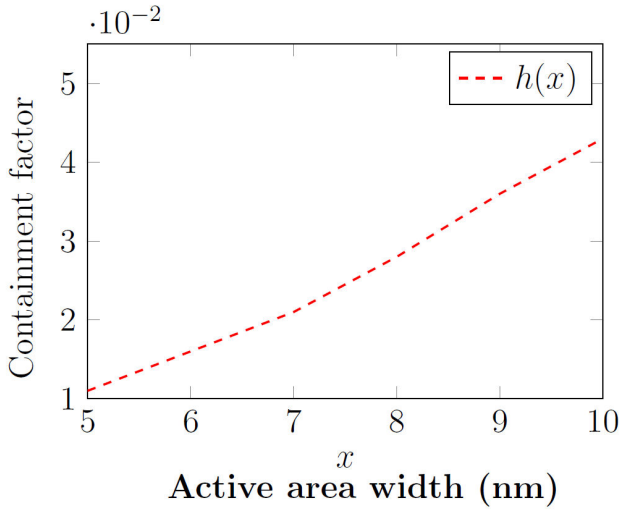

FIGURE 14. Change of the confinement factor as a function of the width of the active zone.

2.6.3. *2.6.3 Containment factor* Γ

We will calculate the confinement factor for the quantum well structure. We will use the $Ga_{0.5}In_{0.5}P$ ternary as an active layer and the $Al_{0.31}Ga_{0.21}In_{0.48}P$ quaternary as a barrier for the following structure (Fig. 13).

a) Confinement factor as a function of well width

Figure 14 shows that the confinement factor of a quantum well threshold structure increases with the well width.

We also note a weak growth of the confinement factor with the aluminum content in the barrier. Note that all the values of the confinement factor are low (max 4% for 10 nm).

2.6.4. *Gain maximal*

The maximum gain will be studied as a function of several parameters such as well width, carrier density, temperature, wavelength for the previous structure (Fig. 13).

a) Maximum gain with a carrier density

The gain increases with the carrier density (Fig. 15). Note that the gain becomes positive and increases from a density

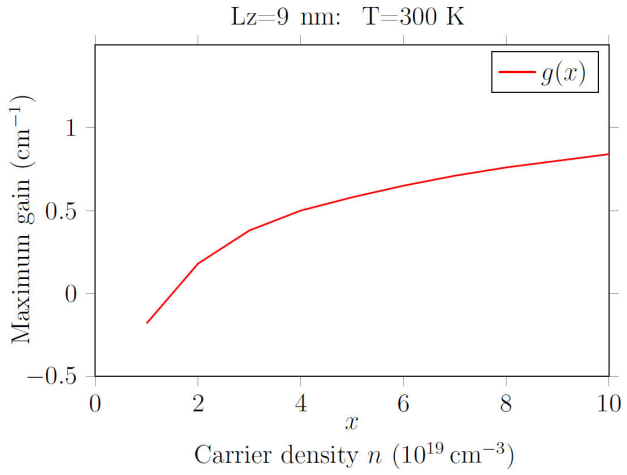

FIGURE 15. Change of maximum gain with an injection.

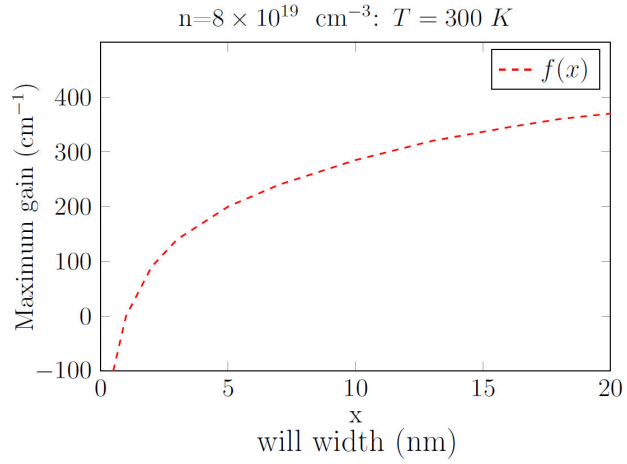

FIGURE 16. Change of maximum gain with a well width.

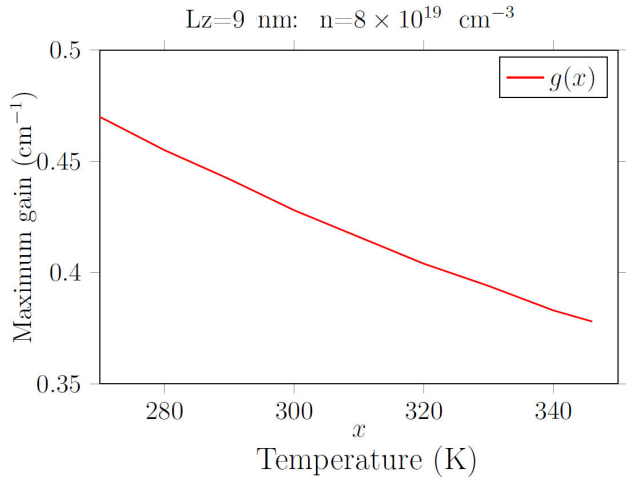

FIGURE 17. Change of maximum gain with a temperature.

equal to 2.858×10^{18} cm^{-3}, which is the transparency density. Remember that transparency density corresponds to zero gain.

b) Maximum gain as a function of well width

Max gain increases with well width (Fig. 16). From a well width equal to 1 nm, this gain is positive.

c) Maximum gain as a function of temperature

Figure 17 shows that temperature has a slight but negative influence on the maximum gain. When the temperature increases from 200 to 300, the maximum gain increases by only 0.5%, so the influence of temperature is negligible.

3. Conclusion

Using the empirical pseudo potential method (EPM) in conjunction with the virtual crystal approximation (VCA), we have examined the electrical characteristics of the $Ga_xIn_{1-x}P$ alloy both with and without accounting for the effects of compositional disorder. Overall, there is good agreement between our findings and the experimental values. The studied material turns out to be a direct bandgap semiconductor for $x < 0.78$ and an indirect bandgap semiconductor for $x > 0.78$. We have calculated the confinement factor for a single quantum well structure. The values obtained are low, and the confinement factor increases with the well width. In the study of the maximum gain, we have found the optimal values relating this maximum gain to the well width. We have also studied the change of the maximum gain with the current density. The maximum gain also depends on the temperature. Finally, this theoretical study allowed us to determine the optimal values for a GaInP/AlGaInP -based quantum well laser.

Declaration of competing interests:

No financial interests or personal relationships that may have influenced the work presented in this article.

Data availability:

The data are available from the corresponding author.

Funding Declaration:

None

Research involving human and animal rights

The article adheres to the ethical principles of the journal and does not contain results of studies involving humans and/or animals.

1. H. Sumitomo *et al*., "High-Power Short-Cavity AlGaInP Laser Diodes," *SEI Technical Review*, **70** (2010) 79. ISSN: 1343-4330.
2. I. Vurgaftman, J. R. Meyer, and L. R. Ram-Mohan, "Band parameters for III–V compound semiconductors and their alloys," *Journal of Applied Physics*, **89** (2001) 5815.
3. V. I. Kozlovsky, S. M. Zhenishbekov, Ya. K. Skasyrsky and M. P. Frolov, High-Power Pulsed, In-Well-Pumped InGaP/AlGaInP Heterostructure Semiconductor Disk Laser, *B. Lebedev Phys. Inst.*, **51** (2024) S191.
4. H. Panwar and J. S. Parmar, Designing of Optical Gain Analysis of Nano-Scale Heterostructure GaInP/AlGaInP Red Laser, *ICIMMI '22: Proceedings of the 4th International Conference on Information Management & Machine Intelligence*, **78** (2023) 1.
5. V. M. Titze, S. Caixeiro, A. Di Falco, M. Schubert and M. C. Gather, "Red-Shifted Excitation and Two-Photon Pumping of Biointegrated GaInP/AlGaInP Quantum Well Microlasers," *ACS Photonics*, **9** (2022) 952.
6. M. U. Anum, H. Usman and A. Shazma, "Epitaxial analysis of GaInP/AlGaInP red light-emitting diodes with ternary AlGaP quantum barriers for quantum efficiency enhancement," *Physica Scripta*, **99** (2024).
7. F. Mauerhoff, H. Wenzel, A. Maaßdorf, D. Martin, K. Paschke and G. Tränkle, "Optimization of high power AlGaInP laser diodes at 626 nm," *Optical and Quantum Electronics*, **56** (2024) 419.
8. S. Adachi, "Band gaps and refractive indices of AlGaAsSb, GaInAsSb, and InPAsSb: Key properties for a variety of the 2–4 μm optoelectronic device applications," *Journal of Applied Physics*, **61** (1987) 4869.
9. M. Levinshtein, S. Rumyantsev and M. Shur (Eds.), *Handbook Series on Semiconductor Parameters*, 2, (World Scientific, 1999). ISBN: 981-02-14120-0.
10. S. J. Lee, T. S. Kwon, K. Nahm and C. K. Kim, Band structure of ternary compound semiconductors beyond the virtual crystal approximation, *Journal of Physics: Condensed Matter*, **2** (1990) 3253.
11. N. Bouarissa, Electronic properties of $Ga_xIn_{1-x}P$ from pseudopotential calculations, *Materials Chemistry and Physics*, **124** (2010) 336.